trajectory AB. Conversely, if $U < c$, the air parcel will fall behind the trough of the wave and curve southeastward, as indicated by AD. By construction, each of the three trajectories is parallel to the initial streamline passing through point A and to the respective later streamlines passing through points B, C, and D. The longest trajectory (AB) corresponds to the highest wind speed.

7.2 Dynamics of Horizontal Flow

Newton's second law states that in each of the three directions in the coordinate system, the acceleration a experienced by a body of mass m in response to a resultant force ΣF is given by

$$a = \frac{1}{m}\sum F \tag{7.6}$$

This relationship describes the motion in an inertial (nonaccelerating) frame of reference. However, it is more generally applicable, provided that *apparent forces* are introduced to compensate for the acceleration of the coordinate system. In a rotating frame of reference two different apparent forces are required: a *centrifugal force* that is experienced by all bodies, irrespective of their motion, and a *Coriolis force* that depends on the relative velocity of the body in the plane perpendicular to the axis of rotation (i.e., in the plane parallel to the equatorial plane).

7.2.1 Apparent Forces

The force per unit mass that is referred to as *gravity* or *effective gravity* and denoted by the symbol g represents the vectorial sum of the true gravitational attraction g* that draws all elements of mass toward Earth's center of mass and the much smaller apparent force called the *centrifugal force* $\Omega^2 R_A$, where Ω is the rotation rate of the coordinate system in radians per second (i.e., s^{-1}) and R_A is the distance from the axis of rotation. The centrifugal force pulls all objects outward from the axis of planetary rotation, as indicated in Fig. 7.6. In mathematical notation,

$$\mathbf{g} = \mathbf{g}^* + \Omega^2 \boldsymbol{R_A}.$$

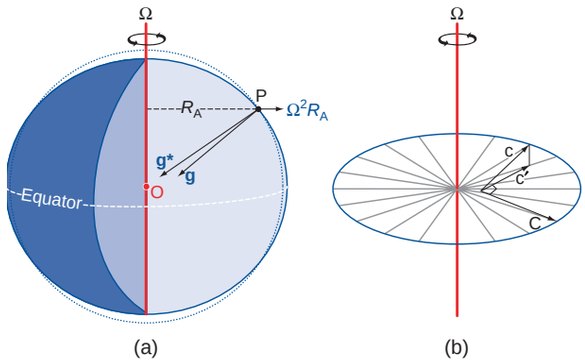

Fig. 7.6 (a) Apparent forces. Effective gravity **g** is the vectorial sum of the true gravitational acceleration **g*** directed toward the center of the Earth O and the *centrifugal force* $\Omega^2 R_A$. The acceleration **g** is normal to a surface of constant geopotential, an oblate spheroid, depicted as the outline of the Earth. The dashed reference line represents a true spherical surface. (b) The Coriolis force C is linearly proportional to **c**′ the component of the relative velocity **c** in the plane perpendicular to the axis of rotation. When viewed from a northern hemisphere perspective, C is directed to the right of **c**′ and lies in the plane perpendicular to the axis of rotation.

Surfaces of constant geopotential Φ, which are normal to **g**, are shaped like oblate spheroids, as indicated by the outline of the Earth in Fig. 7.6. Because the surface of the oceans and the large-scale configuration of the Earth's crust are incapable of resisting any sideways pull of effective gravity, they have aligned themselves with surfaces of constant geopotential. A body rotating with the Earth has no way of separately sensing the gravitational and centrifugal components of effective gravity. Hence, the $\Omega^2 \boldsymbol{R_A}$ term is incorporated into **g** in the equations of motion.

An object moving with velocity **c** in the plane perpendicular to the axis of rotation experiences an additional apparent force called the *Coriolis*[2] *force* $-2\Omega \times \mathbf{c}$. This apparent force is also in the plane perpendicular to the axis of rotation, and it is directed transverse to the motion in accordance with the right hand rule (i.e., if the rotation is counterclockwise when viewed from above, the force is directed to the right of **c** and vice versa).

When the forces and the motions are represented in a spherical coordinate system, the horizontal component of the Coriolis force arising from the

[2] **G. G. de Coriolis** (1792–1843) French engineer, mathmatician, and physicist. Gave the first modern definition of kinetic energy and work. Studied motions in rotating systems.

horizontal motion $\mathbf{V}$ can be written in vectorial form as

$$\mathbf{C} = -f\mathbf{k} \times \mathbf{V} \tag{7.7}$$

where f, the so-called *Coriolis parameter*, is equal to $2\Omega \sin \phi$ and $\mathbf{k}$ is the local vertical unit vector, defined as positive upward. The $\sin \phi$ term in f appropriately scales the Coriolis force to account for the fact that the local vertical unit vector $\mathbf{k}$ is parallel to the axis of rotation Ω only at the poles. Accordingly, the Coriolis force in the horizontal equation of motion increases with latitude from zero on the equator to $2\Omega V$ at the poles, where V is the (scalar) horizontal wind speed. The Coriolis force is directed toward the right of the horizontal velocity vector in the northern hemisphere and to the left of it in the southern hemisphere. On Earth

$$\Omega \equiv 2\pi \text{ rad day}^{-1} = 7.292 \times 10^{-5} \text{ s}^{-1}$$

where *day* in this context refers to the *sidereal day*,[3] which is 23 h 56 min in length.

7.1 Experiment in a Dish

The role of the Coriolis force in a rotating coordinate system can be demonstrated in laboratory experiments. Here we describe an experiment that makes use of a special apparatus in which the centrifugal force is incorporated into the vertical force called gravity, as it is on Earth. The apparatus consists of a shallow dish, rotating about its axis of symmetry as shown in Fig. 7.7. The rotation rate Ω is tuned to the concavity of the dish such that at any given radius the outward-directed centrifugal force exactly balances the inward-directed component of gravity along the sloping surface of the dish; that is

$$g\frac{dz}{dr} = \Omega^2 r$$

where z is the height of the surface above some arbitrary reference level, r is the radius, and Ω is the rotation rate of the dish. Integrating from the center out to radius r yields the parabolic surface

$$z = \frac{\Omega^2 r^2}{2g} + \textit{constant}$$

The constant of integration is chosen to make $z = 0$ the level of the center of the dish.

Consider the horizontal trajectory of an idealized frictionless marble rolling around in the dish, as represented in both a fixed (inertial) frame of reference and in a frame of reference rotating with the dish. (To view the motion in the rotating frame of reference, the video camera is mounted on the turntable.)

In the fixed frame of reference the differential equation governing the horizontal motion of the marble is

$$\frac{d^2 r}{dt^2} = -\Omega^2 r$$

It follows from the form of this differential equation that the marble will execute elliptical trajectories, symmetric about the axis of rotation, with

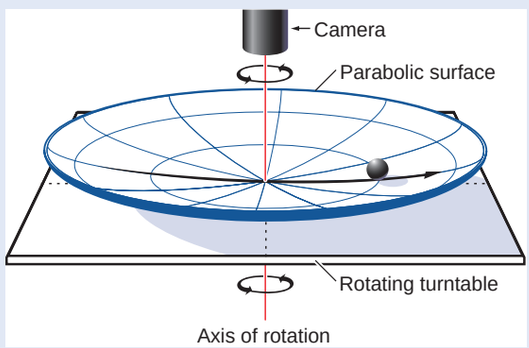

Fig. 7.7 Setup for the rotating dish experiment. Radius r is distance from the axis of rotation. Angular velocity Ω is the rotation rate of the dish. See text for further explanation.

Continued on next page

[3] The time interval between successive transits of a star over a meridian.

7.1 Continued

period $2\pi/\Omega$, which exactly matches the period of rotation of the dish. The shape and orientation of these trajectories will depend on the initial position and velocity of the marble. In this example, the marble is released at radius $r = r_0$ with no initial velocity. After the marble is released it rolls back and forth, like the tip of a pendulum, along the straight line pictured in Fig. 7.7, with a period equal to $2\pi/\Omega$, the same as the period of rotation of the dish. This oscillatory solution is represented by the equation

$$r = r_0 \cos \Omega t$$

where t is time and radius r is defined as positive on the side of the dish from which the marble is released and negative on the other side. The velocity of the marble along its pendulum-like trajectory

$$\frac{dr}{dt} = -\Omega r_0 \sin \Omega t$$

is largest at the times when it passes through the center of the dish at $t = \pi/2,\ 3\pi/2 \ldots$, and the marble is motionless for an instant at $t = \pi,\ 2\pi \ldots$ when it reverses direction at the outer edge of its trajectory.

In the rotating frame of reference the only force in the horizontal equation of motion is the Coriolis force, so the governing equation is

$$\frac{d\mathbf{c}}{dt} = -2\Omega\mathbf{k} \times \mathbf{c}$$

where $\mathbf{c}$ is the velocity of the marble and $\mathbf{k}$ is the vertical (normal to the surface of the dish) unit vector. Because $d\mathbf{c}/dt$ is perpendicular to $\mathbf{c}$, it follows that c, the speed of the marble as it moves along its trajectory in the rotating frame of reference, must be constant. The direction of the forward motion of the marble is changing with time at the uniform rate 2Ω, which is exactly twice the rate of rotation of the dish. Hence, the marble executes a circular orbit called an *inertia circle*, with period $2\pi/2\Omega = \pi/\Omega$ (i.e., half the period of rotation of the dish), with circumference $c\ (\pi/\Omega)$, and radius $c\ (\pi/\Omega)/2\pi = c/2\Omega$. Because $d\mathbf{c}/dt$ is to the right of $\mathbf{c}$, it follows that the marble rolls clockwise, i.e., in the opposite sense as the rotation of the dish.

As in the fixed frame of reference, the trajectory of the marble depends on its initial position and relative motion. Because the marble is released at radius r_0 with no initial motion in the fixed frame of reference, it follows that its speed in the rotating frame of reference is $c = \Omega r_0$, and thus the radius of the inertia circle is $\Omega r_0/2\Omega = r_0/2$. It follows that the marble passes through the center of the dish at the midpoint of its trajectory around the inertia circle.

The motion of the marble in the fixed and rotating frames of reference is shown in Fig. 7.8. The rotating dish is represented by the large circle. The point of release of the marble is labeled **0** and appears at the top of the diagram rather than on the left side of the dish as in Fig. 7.7. The pendulum-like trajectory of the marble in the fixed frame of reference is represented by the straight

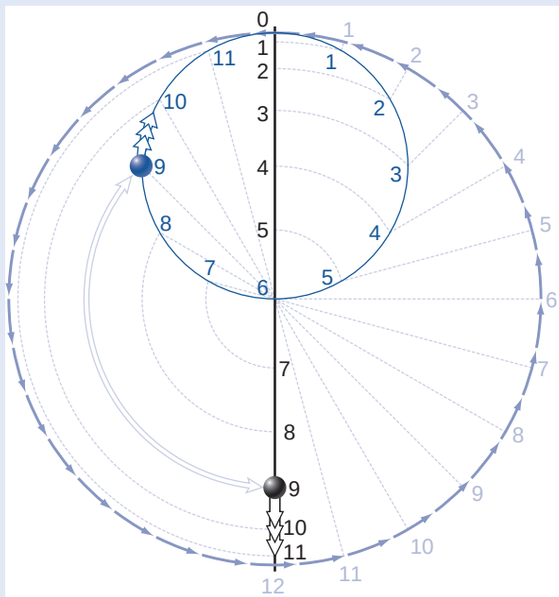

Fig. 7.8 Trajectories of a frictionless marble in fixed (black) and rotating (blue) frames of reference. Numbered points correspond to positions of the marble at various times after it is released at point **0**. One complete rotation of the dish corresponds to one swing back and forth along the straight vertical black line in the fixed frame of reference and two complete circuits of the marble around the blue inertia circle in the rotating frame of reference. The light lines are reference lines. See text for further explanation.

7.1 Continued

black vertical line passing through the center of the dish. Successive positions along the trajectory at equally spaced time intervals are represented by numbers: point **1** represents the position of the marble after 1/24 of the period of rotation of the dish, point **12** after one-half period of rotation, etc. Hence, the numerical values assigned to the points are analogous to the 24 h of the day on a rotating planet. Note that the spacing between successive points is largest near the middle of the pendulum-like trajectory, where the marble is rolling fastest.

The position of the marble in the rotating (blue) frame of reference can be located at any specified time without invoking the Coriolis force simply by subtracting the displacement of the dish from the displacement of the marble in the fixed frame of reference. For example, to locate the marble after one-eighth rotation of the dish, we rotate point **3** clockwise (i.e., in the direction opposite to the rotation of the dish) one-eighth of the way around the circle; point **9** needs to be rotated three-eighths of the way around the circle, and so forth. The rotated points map out the trajectory of the marble in the rotating frame of reference: an inertia circle with a period equal to one-half revolution of the dish (i.e., 12 "hours"). In Fig. 7.8 the marble is pictured at 9 o'clock on the 24-hour clock in the two frames of reference.

Alternatively, the inertia circle can be constructed by first rotating the marble backward (clockwise) from its point of release to subtract the rotation of the dish and then moving the marble radially the appropriate distance along its pendulum-like trajectory. Reference lines for performing these operations are shown in Fig. 7.8. Examples of trajectories for two other sets of initial conditions are presented in Exercise 7.14.

7.2.2 Real Forces

The real forces that enter into the equations of motion are *gravity*, the *pressure gradient force*, and *frictional force* exerted by neighboring air parcels or adjacent surfaces.

a. The pressure gradient force

The vertical component of the pressure gradient force (per unit mass) $-(1/\rho)\partial p/\partial z$ has already been introduced in the context of the hydrostatic equation. The horizontal component of the pressure gradient force is given by the analogous expression

$$\mathbf{P} \equiv -\frac{1}{\rho}\nabla p \tag{7.8a}$$

or, in component form,

$$P_x = -\frac{1}{\rho}\frac{\partial p}{\partial x}; \quad P_y = -\frac{1}{\rho}\frac{\partial p}{\partial y} \tag{7.8b}$$

The pressure gradient force is directed down the horizontal pressure gradient ∇p from higher toward lower pressure. Making use of the hydrostatic equation (3.17) and the definitions of geopotential (3.20) and geopotential height (3.22), the horizontal pressure gradient force can be expressed in the alternative forms

$$\mathbf{P} \equiv -g\nabla z = -g_0\nabla Z = -\nabla\Phi \tag{7.9}$$

where the gradients of geometric height, geopotential height, and geopotential are defined on sloping pressure surfaces. Hence, the pressure gradient force can be interpreted as the component of effective gravity g in the plane of the pressure surface, analogous to the "downhill" force on a ball rolling on a sloping surface. Pressure surfaces exhibit typical slopes on the order of 100 m per thousand kilometers, or 1 in 10^4. Hence, the horizontal component of the pressure gradient force is roughly four orders of magnitude smaller than the vertical component; i.e., it is on the order of 10^{-3} m s^{-2}.

The pressure field on weather charts is typically represented by a set of contours plotted at regularly spaced intervals as in Fig. 1.19. The lines that are used to depict the distribution of pressure on geopotential height surfaces are referred to as *isobars*, and the lines used to depict the distribution of geopotential height on pressure surfaces are referred to as *geopotential height contours*. Exercise 3.3 demonstrates that, to a close approximation, isobars on a constant geopotential surface (e.g., sea level) can be converted into geopotential height contours on a nearby pressure surface simply by relabeling them using a constant of proportionality

based on the hypsometric equation (3.29). For example, near sea level, where atmospheric pressure decreases with height at a rate of ~1 hPa per 8 m, the conventional 4-hPa contour interval for isobars of sea-level pressure is approximately equivalent to a 30-m contour interval for geopotential height contours on a specified pressure surface. It follows that (7.8) and (7.9) yield virtually identical distributions of **P**.

In the oceans the horizontal pressure gradient force is due to both the gradient in sea level on a surface of constant geopotential and horizontal gradients in the density of the overlying water in the column. Near the ocean surface this force is primarily associated with the horizontal gradient in sea level. The topography of sea level is difficult to estimate in an absolute sense from observations because Earth's *geoid* (i.e., geopotential field) exhibits nonellipsoidal irregularities of its own that have more to do with plate tectonics than with oceanography. Temporal variations in sea level relative to Earth's much more slowly evolving geoid are clearly revealed by satellite altimetry.

b. The frictional force

The frictional force (per unit mass) is given by

$$\mathbf{F} = -\frac{1}{\rho}\frac{\partial \tau}{\partial z} \tag{7.10}$$

where τ represents the vertical component of the *shear stress* (i.e., the rate of vertical exchange of horizontal momentum) in units of N m^{-2} due to the presence of smaller, unresolved scales of motion.[4] Vertical exchanges of momentum usually act to smooth out the vertical profile of **V**. The rate of vertical mixing that is occurring at any particular level and time depends on the strength of the vertical wind shear $\partial \mathbf{V}/\partial z$ and on the intensity of the unresolved motions, as discussed in Chapter 9. In the free atmosphere, above the boundary layer, the frictional force is much smaller than the pressure gradient force and the Coriolis force. However, within the boundary layer the frictional force is comparable in magnitude to the other terms in the horizontal equation of motion and needs to be taken into account.

The shear stress τ_s at the Earth's surface is in the opposing direction to the surface wind vector $\mathbf{V}_s$ (i.e., it is a "drag" on the surface wind) and can be approximated by the empirical relationship

$$\tau_s = -\rho C_D \mathbf{V}_s V_s \tag{7.11}$$

where ρ is the density of the air, C_D is a dimensionless *drag coefficient*, the magnitude of which varies with the roughness of the underlying surface and the static stability, $\mathbf{V}_s$ is the surface wind vector, and V_s is the (scalar) surface wind speed. Within the lowest few tens of meters of the atmosphere, the stress decreases with height without much change in direction. Hence, within this so-called *surface layer*, the frictional force $\mathbf{F}_s = -\partial\tau/\partial z$ is directed opposite to $\mathbf{V}_s$ and is referred to as *frictional drag*.

7.2.3 The Horizontal Equation of Motion

The horizontal component of (7.6), written in vectorial form, per unit mass, is

$$\frac{d\mathbf{V}}{dt} = \mathbf{P} + \mathbf{C} + \mathbf{F} \tag{7.12}$$

where $d\mathbf{V}/dt$ is the Lagrangian time derivative of the horizontal velocity component experienced by an air parcel as it moves about in the atmosphere. Substituting for **C** from (7.7) and for **P** from (7.8a) we obtain

$$\frac{d\mathbf{V}}{dt} = -\frac{1}{\rho}\nabla p - f\mathbf{k} \times \mathbf{V} + \mathbf{F} \tag{7.13a}$$

or, in component form on a tangent plane (i.e., neglecting smaller terms that arise due to the curvature of the coordinate system),

$$\begin{aligned} \frac{du}{dt} &= -\frac{1}{\rho}\frac{\partial p}{\partial x} + fv + F_x, \\ \frac{dv}{dt} &= -\frac{1}{\rho}\frac{\partial p}{\partial y} - fu + F_y \end{aligned} \tag{7.13b}$$

The density dependence can be eliminated by substituting for **P** using (7.9) instead of (7.8), which yields

$$\frac{d\mathbf{V}}{dt} = -\nabla\Phi - f\mathbf{k} \times \mathbf{V} + \mathbf{F} \tag{7.14}$$

[4] The contributions of the corresponding horizontal exchanges of momentum to **F** do not need to be considered because the horizontal gradients are much smaller than the vertical gradients.

In (7.13a) the horizontal wind field is defined on surfaces of constant geopotential so that $\nabla\Phi = 0$, whereas in (7.14) it is defined on constant pressure surfaces so that $\nabla p = 0$. However, pressure surfaces are sufficiently flat that the **V** fields on a geopotential surface and a nearby pressure surface are very similar.

7.2.4 The Geostrophic Wind

In large-scale wind systems such as baroclinic waves and extratropical cyclones, typical horizontal velocities are on the order of $10\ \mathrm{m\ s^{-1}}$ and the timescale over which individual air parcels experience significant changes in velocity is on the order of a day or so ($\sim 10^5$ s). Thus a typical parcel acceleration $d\mathbf{V}/dt$ is $\sim 10\ \mathrm{m\ s^{-1}}$ per 10^5 s or $10^{-4}\ \mathrm{m\ s^{-2}}$. In middle latitudes, where $f \sim 10^{-4}\ \mathrm{s^{-1}}$, an air parcel moving at a speed of $10\ \mathrm{m\ s^{-1}}$ experiences a Coriolis force per unit mass **C** $\sim 10^{-3}\ \mathrm{m\ s^{-2}}$, about an order of magnitude larger than the typical horizontal accelerations of air parcels.

In the free atmosphere, where the frictional force is usually very small, the only term that is capable of balancing the Coriolis force **C** is the pressure gradient force **P**. Thus, to within about 10%, in middle and high latitudes, the horizontal equation of motion (7.14) is closely approximated by

$$f\mathbf{k} \times \mathbf{V} \simeq -\nabla\Phi$$

Making use of the vector identity

$$\mathbf{k} \times (\mathbf{k} \times \mathbf{V}) = -\mathbf{V}$$

it follows that

$$\mathbf{V} \simeq \frac{1}{f}(\mathbf{k} \times \nabla\Phi)$$

For any given horizontal distribution of pressure on geopotential surfaces (or geopotential height on pressure surfaces) it is possible to define a *geostrophic*[5] *wind field* $\mathbf{V}_g$ for which this relationship is exactly satisfied:

$$\mathbf{V}_g \equiv \frac{1}{f}(\mathbf{k} \times \nabla\Phi) \tag{7.15a}$$

or, in component form,

$$u_g = -\frac{1}{f}\frac{\partial\Phi}{\partial y}, \quad v_g = \frac{1}{f}\frac{\partial\Phi}{\partial x} \tag{7.15b}$$

or, in natural coordinates,

$$V_g = -\frac{1}{f}\frac{\partial\phi}{\partial n} \tag{7.15c}$$

where V_g is the scalar geostrophic wind speed and n is the direction normal to the isobars (or geopotential height contours), pointing toward higher values.

The balance of horizontal forces implicit in the definition of the geostrophic wind (for a location in the northern hemisphere) is illustrated in Fig. 7.9. In order for the Coriolis force and the pressure gradient force to balance, the geostrophic wind must blow parallel to the isobars, leaving low pressure to the left. In either hemisphere, the geostrophic wind field circulates cyclonically around a center of low pressure and vice versa, as in Fig. 1.14, justifying the identification of local pressure minima with cyclones and local pressure maxima with anticyclones. The tighter the spacing of the isobars or geopotential height contours, the stronger the Coriolis force required to balance the pressure gradient force and hence, the higher the speed of the geostrophic wind.

7.2.5 The Effect of Friction

The three-way balance of forces required for flow in which $d\mathbf{V}/dt = 0$ in the northern hemisphere in the presence of friction at the Earth's surface is illustrated in Fig. 7.10. As in Fig. 7.9, **P** is directed normal

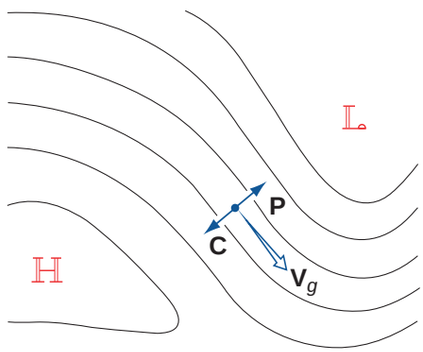

Fig. 7.9 The geostrophic wind V_g and its relationship to the horizontal pressure gradient force P and the Coriolis force C in the northern hemisphere.

[5] From the Greek: *geo* (Earth) and *strophen* (to turn)

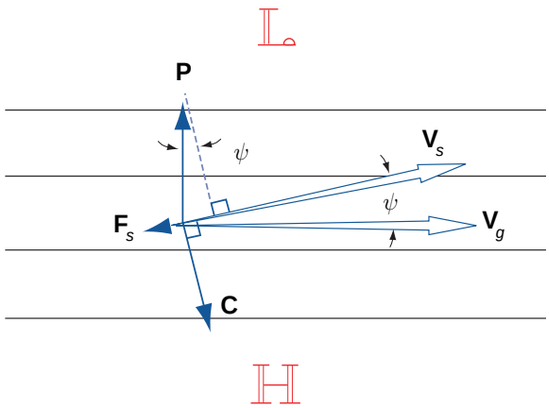

Fig. 7.10 The three-way balance of forces required for steady surface winds in the presence of the frictional drag force F in the northern hemisphere. Solid lines represent isobars or geopotential height contours on a weather chart.

to the isobars, **C** is directed to the right of the horizontal velocity vector $\mathbf{V}_s$, and, consistent with (7.11), $\mathbf{F}_s$ is directed opposite to $\mathbf{V}_s$. The angle ψ between $\mathbf{V}_s$ and $\mathbf{V}_g$ is determined by the requirement that the component of **P** in the forward direction of $\mathbf{V}_s$ must be equal to the magnitude of the drag $\mathbf{F}_s$, and the wind speed V_s is determined by the requirement that **C** be just large enough to balance the component of **P** in the direction normal to $\mathbf{V}_s$; i.e.,

$$fV_s = |\mathbf{P}| \cos\psi$$

It follows that $|\mathbf{C}| < |\mathbf{P}|$ and, hence, the scalar wind speed $V_s = |\mathbf{C}|/f$ must be smaller than $V_g = |\mathbf{P}|/f$. The stronger the frictional drag force $\mathbf{F}_s$, the larger the angle ψ between $\mathbf{V}_g$ and $\mathbf{V}_s$ and the more *subgeostrophic* the surface wind speed $\mathbf{V}_s$. The cross-isobar flow toward lower pressure, referred to as the *Ekman*[6] *drift*, is clearly evident on surface charts, particularly over rough land surfaces. That the winds

Fig. 7.11 The force balance associated with Ekman drift in the northern hemisphere oceans. The frictional force F is in the direction of the surface wind vector. In the southern hemisphere (not shown) the Ekman drift is to the left of the surface wind vector.

usually blow nearly parallel to the isobars in the free atmosphere indicates that the significance of the frictional drag force is largely restricted to the boundary layer, where small-scale turbulent motions are present.

The same shear stress that acts as a drag force on the surface winds exerts a forward pull on the surface waters of the ocean, giving rise to *wind-driven currents*. If the ocean surface coincided with a surface of constant geopotential, the balance of forces just below the surface would consist of a two-way balance between the forward pull of the surface wind and the backward pull of the Coriolis force induced by the Ekman drift, as shown in Fig. 7.11. Although the large scale surface currents depicted in Fig. 2.4 tend to be in geostrophic balance and oriented roughly parallel to the mean surface winds, the Ekman drift, which is directed normal to the surface winds, has a pronounced effect on horizontal transport of near-surface water and sea-ice, and it largely controls the distribution of upwelling, as discussed in Section 7.3.4. Ekman drift is largely confined to the topmost 50 m of the oceans.

7.2.6 The Gradient Wind

The centripetal accelerations observed in association with the curvature of the trajectories of air parcels tend to be much larger than those associated with

[6] **V. Walfrid Ekman** (1874–1954) Swedish oceanographer. Ekman was introduced to the problem of wind-driven ocean circulation when he was a student working under the direction of Professor Vilhelm Bjerknes.[7] Fridtjof Nansen had approached Bjerknes with a remarkable set of observations of winds and ice motions taken during the voyage of the *Fram*, for which he sought an explanation. Nansen's observations and Ekman's mathematical analysis are the foundations of the theory of the wind-driven ocean circulation.

[7] **Vilhelm Bjerknes** (1862–1951) Norwegian physicist and one of the founders of the science of meteorology. Held academic positions at the universities of Stockholm, Bergen, Leipzig, and Kristiania (renamed Oslo). Proposed in 1904 that weather prediction be regarded as an initial value problem that could be solved by integrating the governing equations forward in time, starting from an initial state determined by current weather observations. Best known for his work at Bergen (1917–1926) where he assembled a small group of dedicated and talented young researchers, including his son Jakob. The most widely recognized achievement of this so-called "Bergen School" was a conceptual framework for interpreting the structure and evolution of extratropical cyclones and fronts that has endured until the present day.

the speeding up or slowing down of air parcels as they move downstream. Hence, when $d\mathbf{V}/dt$ is large, its scalar magnitude can be approximated by the centripetal acceleration V^2/R_T, where R_T is the local radius of curvature of the air trajectories.[8] Hence, the horizontal equation of motion reduces to the balance of forces in the direction transverse to the flow, i.e.,

$$\mathbf{n}\frac{V^2}{R_T} = -\nabla\Phi - f\mathbf{k}\times\mathbf{V} \tag{7.16}$$

The signs of the terms in this three-way balance depend on whether the curvature of the trajectories is cyclonic or anticyclonic, as illustrated in Fig. 7.12. In the cyclonic case, the outward centrifugal force (the mirror image of the centripetal acceleration) reinforces the Coriolis force so that a balance can be achieved with a wind speed smaller than would be required if the Coriolis force were acting alone. In flow through sharp troughs, where the curvature of the trajectories is cyclonic, the observed wind speeds at the jet stream level are often smaller, by a factor of two or more, than the geostrophic wind speed implied by the spacing of the isobars. For the anticyclonically curved trajectory on the right in Fig. 7.12 the centrifugal force opposes the Coriolis force, necessitating a *supergeostrophic* wind speed in order to achieve a balance.

The wind associated with a three-way balance between the pressure gradient and Coriolis and centrifugal forces is called the *gradient wind*. The solution of (7.16), which yields the speed of the gradient wind can be written in the form

$$V_{gr} = \frac{1}{f}\left(|\nabla\Phi| + \frac{V_{gr}^2}{R_T}\right) \tag{7.17}$$

and solved using the quadratic formula. From Fig. 7.12, it can be inferred that R_T should be specified as positive if the curvature is cyclonic and negative if the curvature is anticyclonic. For the case of anticyclonic curvature, a solution exists when

$$|\nabla\Phi| \le \frac{f^2|R_T|}{4}$$

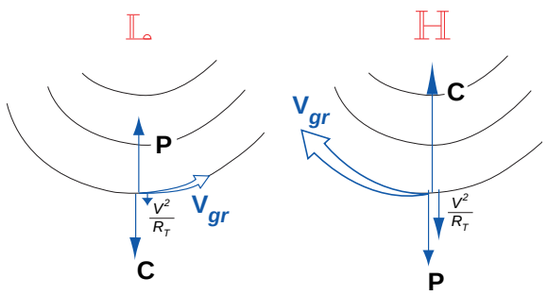

Fig. 7.12 The three-way balance involving the horizontal pressure gradient force P, the Coriolis force C, and the centrifugal force $|V|^2/R_T$ in flow along curved trajectories in the northern hemisphere. (Left) Cyclonic flow. (Right) Anticyclonic flow.

7.2.7 The Thermal Wind

Just as the geostrophic wind bears a simple relationship to $\nabla\Phi$, the vertical shear of the geostrophic wind bears a simple relationship to ∇T. Writing the geostrophic equation (7.15a) for two different pressure surfaces and subtracting, we obtain an expression for the vertical wind shear in the intervening layer

$$(\mathbf{V}_g)_2 - (\mathbf{V}_g)_1 = \frac{1}{f}\mathbf{k}\times\nabla(\Phi_2 - \Phi_1) \tag{7.18}$$

In terms of geopotential height

$$(\mathbf{V}_g)_2 - (\mathbf{V}_g)_1 = \frac{g_0}{f}\mathbf{k}\times\nabla(Z_2 - Z_1) \tag{7.19a}$$

or in component form,

$$\begin{aligned}(u_g)_2 - (u_g)_1 &= -\frac{g_0}{f}\frac{\partial(Z_2 - Z_1)}{\partial y},\\ (v_g)_2 - (v_g)_1 &= \frac{g_0}{f}\frac{\partial(Z_2 - Z_1)}{\partial x}\end{aligned} \tag{7.19b}$$

This expression, known as the *thermal wind equation*, states that the vertically averaged vertical shear of the geostrophic wind within the layer between any two pressure surfaces is related to the horizontal gradient of thickness of the layer in the same manner in which geostrophic wind is related to geopotential height. For example, in the northern hemisphere the *thermal wind*

[8] In estimating the radius of curvature in the gradient wind equation it is important to keep in mind the distinction between *streamlines* and *trajectories*, as explained in Section 7.1.4.

(namely the vertical shear of the geostrophic wind) "blows" parallel to the thickness contours, leaving low thickness to the left. Incorporating the linear proportionality between temperature and thickness in the hypsometric equation (3.29), the thermal wind equation can also be expressed as a linear relationship between the vertical shear of the geostrophic wind and the horizontal temperature gradient.

$$(\mathbf{V}_g)_2 - (\mathbf{V}_g)_1 = \left(\frac{R}{f}\ln\frac{p_1}{p_2}\right)\mathbf{k} \times \nabla(\overline{T}) \qquad (7.20)$$

where $\overline{T}$ is the vertically averaged temperature within the layer.

To explore the implications of the thermal wind equation, consider first the special case of an atmosphere that is characterized by a total absence of horizontal temperature (thickness) gradients. In such a *barotropic*[9] atmosphere $\nabla T = 0$ on constant pressure surfaces. Because the thickness of the layer between any pair of pressure surfaces is horizontally uniform, it follows that the geopotential height contours on various pressure surfaces can be neatly stacked on top of one another, like a set of matched dinner plates. It follows that the direction and speed of the geostrophic wind must be independent of height.

Now let us consider an atmosphere with horizontal temperature gradients subject to the constraint that the thickness contours be everywhere parallel to the geopotential height contours. For historical reasons, such a flow configuration is referred to as *equivalent barotropic*. It follows from the thermal wind equation that the vertical wind shear in an equivalent barotropic atmosphere must be parallel to the wind itself so the direction of the geostrophic wind does not change with height, just as in the case of a pure barotropic atmosphere. However, the slope of the pressure surfaces and hence the speed of the geostrophic wind may vary from level to level in association with thickness variations in the direction normal to height contours, as illustrated in Fig. 7.13.

In an equivalent barotropic atmosphere, the isobars and isotherms on horizontal maps have the same shape. If the highs are warm and the lows are cold, the amplitude of features in the pressure field and the speed of the geostrophic wind increase with height. If the highs are cold and the lows are warm, the situation is just the opposite; features in the pressure and geostrophic wind field tend to weaken with height and the wind may even reverse direction if the temperature anomalies extend through a deep enough layer, as in Fig. 7.13b. The zonally averaged zonal wind and temperature cross sections shown in Fig. 1.11 are related in a manner consistent with Fig. 7.13. Wherever temperature decreases with increasing latitude, the zonal wind becomes (relatively) more westerly with increasing height, and vice versa.

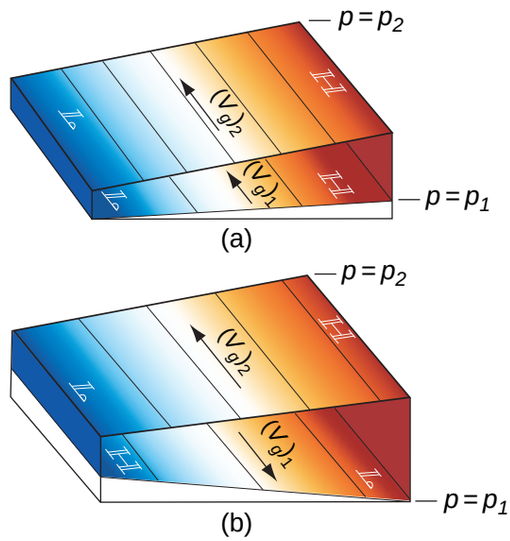

Fig. 7.13 The change of the geostrophic wind with height in an equivalent barotropic flow in the northern hemisphere: (a) V_g increasing with height within the layer and (b) V_g reversing direction. The temperature gradient within the layer is indicated by the shading: blue (cold) coincides with low thickness and tan (warm) with high thickness.

Exercise 7.3 During winter in the troposphere ~30° latitude, the zonally averaged temperature gradient is ~0.75 K per degree of latitude (see Fig. 1.11) and the zonally averaged component of the geostrophic wind at the Earth's surface is close to zero. Estimate the mean zonal wind at the jet stream level, ~250 hPa.

Solution: Taking the zonal component of (7.20) and averaging around a latitude circle yields

$$[u_g]_{250} - [u_g]_{1000} = -\frac{R}{2\Omega\sin\phi}\frac{\partial[T]}{\partial y}\ln\frac{1000}{250}$$

[9] The term barotropic is derived from the Greek *baro*, relating to pressure, and *tropic*, changing in a specific manner: that is, in such a way that surfaces of constant pressure are coincident with surfaces of constant temperature or density.

Noting that $[u_g]_{1000} \simeq 0$ and $R \simeq R_d$

$$[u_g]_{250} = -\frac{287 \text{ J deg}^{-1} \text{ kg}^{-1}}{2 \times 7.29 \times 10^{-5} \text{ s}^{-1} \sin 30^\circ} \times \ln 4 \times \frac{-0.75 \text{ K}}{1.11 \times 10^5 \text{ m}} = 36.8 \text{ m s}^{-1},$$

in close agreement with Fig. 1.11. ■

In a fully *baroclinic atmosphere*, the height and thickness contours intersect one another so that the geostrophic wind exhibits a component normal to the isotherms (or thickness contours). This geostrophic flow across the isotherms is associated with *geostrophic temperature advection. Cold advection* denotes flow across the isotherms from a colder to a warmer region, and vice versa.

Typical situations corresponding to cold and warm advection in the northern hemisphere are illustrated in Fig. 7.14. On the pressure level at the bottom of the layer the geostrophic wind is from the west so the height contours are oriented from west to east, with lower heights toward the north. Higher thickness lies toward the east in the cold advection case (Fig. 7.14a) and toward the west in the warm advection case (Fig. 7.14b).[10]

The upper level geostrophic wind vector $\mathbf{V}_{g2}$ blows parallel to these upper-level contours. Just as the upper level geopotential height is the algebraic sum of the lower level geopotential height Z_1 plus the thickness Z_T, the upper level geostrophic wind vector $\mathbf{V}_{g2}$ is the vectorial sum of the lower level geostrophic wind $\mathbf{V}_{g1}$ plus the thermal wind $\mathbf{V}_T$. Hence, *thermal wind* is to *thickness* as *geostrophic wind* is to *geopotential height*.

From Fig. 7.14 it is apparent that cold advection is characterized by *backing* (cyclonic rotation) of the geostrophic wind vector with height and warm advection is characterized by *veering* (anticyclonic rotation). By experimenting with other configurations of height and thickness contours, it is readily verified that this relationship holds, regardless of the direction of the geostrophic wind at the bottom of the layer or the orientation of the isotherms, and it holds for the southern hemisphere as well.

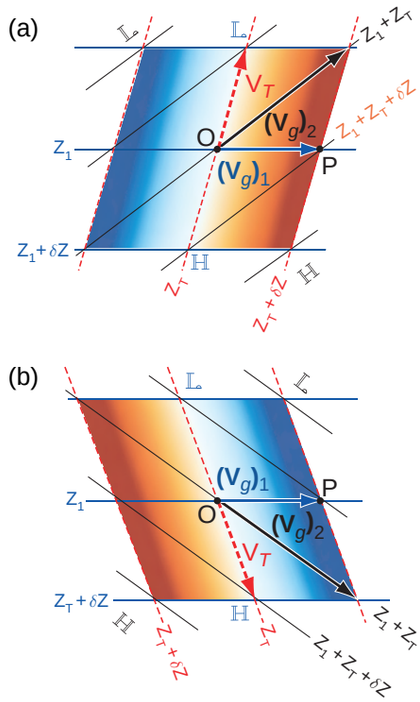

Fig. 7.14 Relationships among isotherms, geopotential height contours, and geostrophic wind in layers with (a) cold and (b) warm advection. Solid blue lines denote the geopotential height contours at the bottom of the layer and solid black lines denote the geopotential height contours at the top of the layer. Red lines represent the isotherms or thickness contours within the layer.

Making use of the thermal wind equation it is possible to completely define the geostrophic wind field on the basis of knowledge of the distribution of $T(x, y, p)$, together with boundary conditions for either $p(x, y)$ or $\mathbf{V}_g(x, y)$ at the Earth's surface or at some other "reference level." Thus, for example, a set of sea-level pressure observations together with an array of closely spaced temperature soundings from satellite-borne sensors constitutes an observing system suitable for determining the three-dimensional distribution of $\mathbf{V}_g$.

[10] Given the distribution of geopotential height Z_1 at the lower level and thickness Z_T, it is possible to infer the geopotential height Z_2 at the upper level by simple addition. For example, the height Z_2 at point O at the center of the diagram is equal to $Z_1 + Z_T$, and at point P it is $Z_1 + (Z_T + \delta Z)$, and so forth. The upper-level height contours (solid black lines) are drawn by connecting intersections with equal values of this sum. If the fields of Z_1, Z_2, and Z_T are all displayed using the same contour interval (say, 60 m), then all intersections between countours will be three-way intersections. In a similar manner, given a knowledge of the geopotential height field at the lower and upper levels, it is possible to infer the thickness field Z_T by subtracting Z_1 from Z_2.